Fundamental physics and chemistry of direct electrochemical oxidation in SOFC

DECO MURI | Colorado School of Mines | University of Maryland | California Institute of Technology

Robert J. Kee, Anthony M. Dean, and Mark T. Lusk
Colorado School of Mines

David G. Goodwin, Sossina M. Haile, and William A. Goddard, III
California Institute of Technology

Gregory S. Jackson, Robert A. Walker, and Bryan W. Eichhorn
University of Maryland, College Park

rjkee@mines.edu
(303) 273-3379

Presented:
SECA Workshop
Asilomar, CA
April 20, 2005

The MURI research seeks to understand the chemical fundamentals of DECO

Important fundamental issues

- Establish elementary kinetics of charge-transfer processes
- Establish elementary kinetics of internal reforming and partial oxidation
- Couple elementary thermal chemistry and electrochemistry
- Determine the chemical routes to deposit formation
- Bridge scales (atomic to fluid flow) to predict cell-level performance

Technical approach

- Develop and apply predictive models across length scales
- Devise and operate experiments that illuminate particular processes
- Use focused experiments to inform, guide, and validate modeling
- Use modeling to help focus and interpret experimentation

Overall objectives

- Develop and validate advanced modeling tools
- Assist the optimal design and development of fuel-cell architectures

Concerted theory and experimentation work to improve understanding the fundamentals

DECO MURI | Colorado School of Mines | University of Maryland | California Institute of Technology

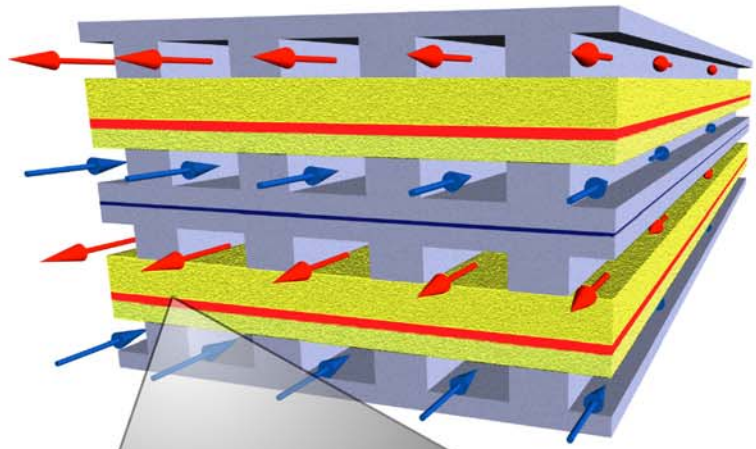

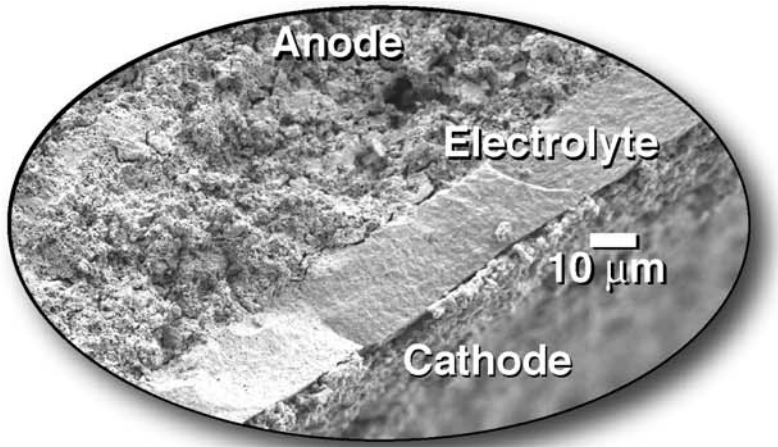

Innovative new materials

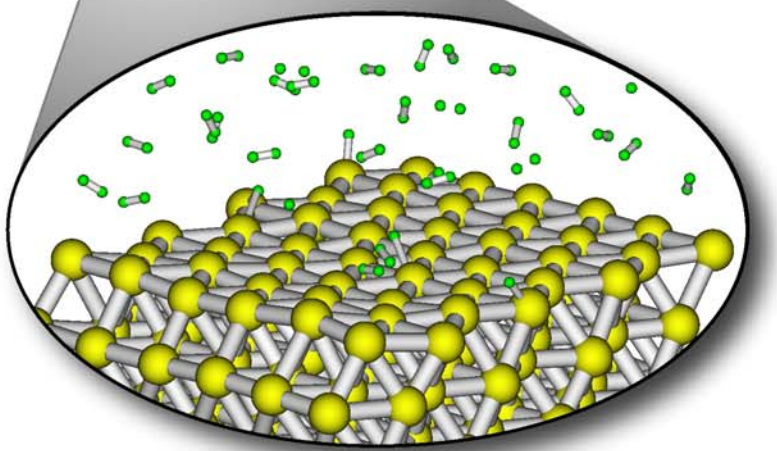

Model across length scales

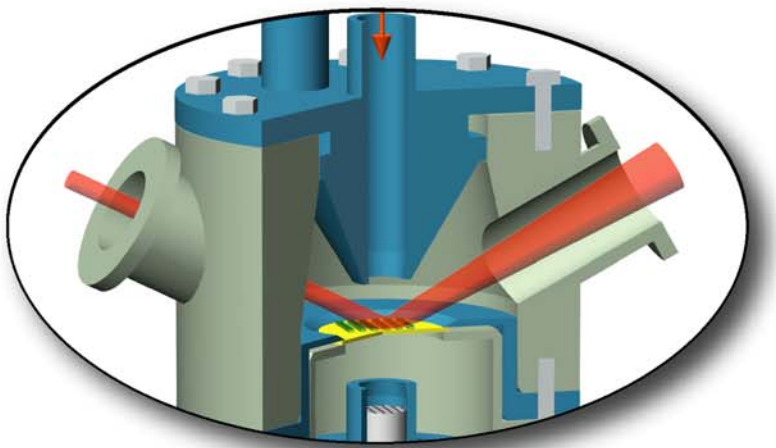

Experiments to isolate physics

Molecular dynamics assists understanding surface chemistry and transport

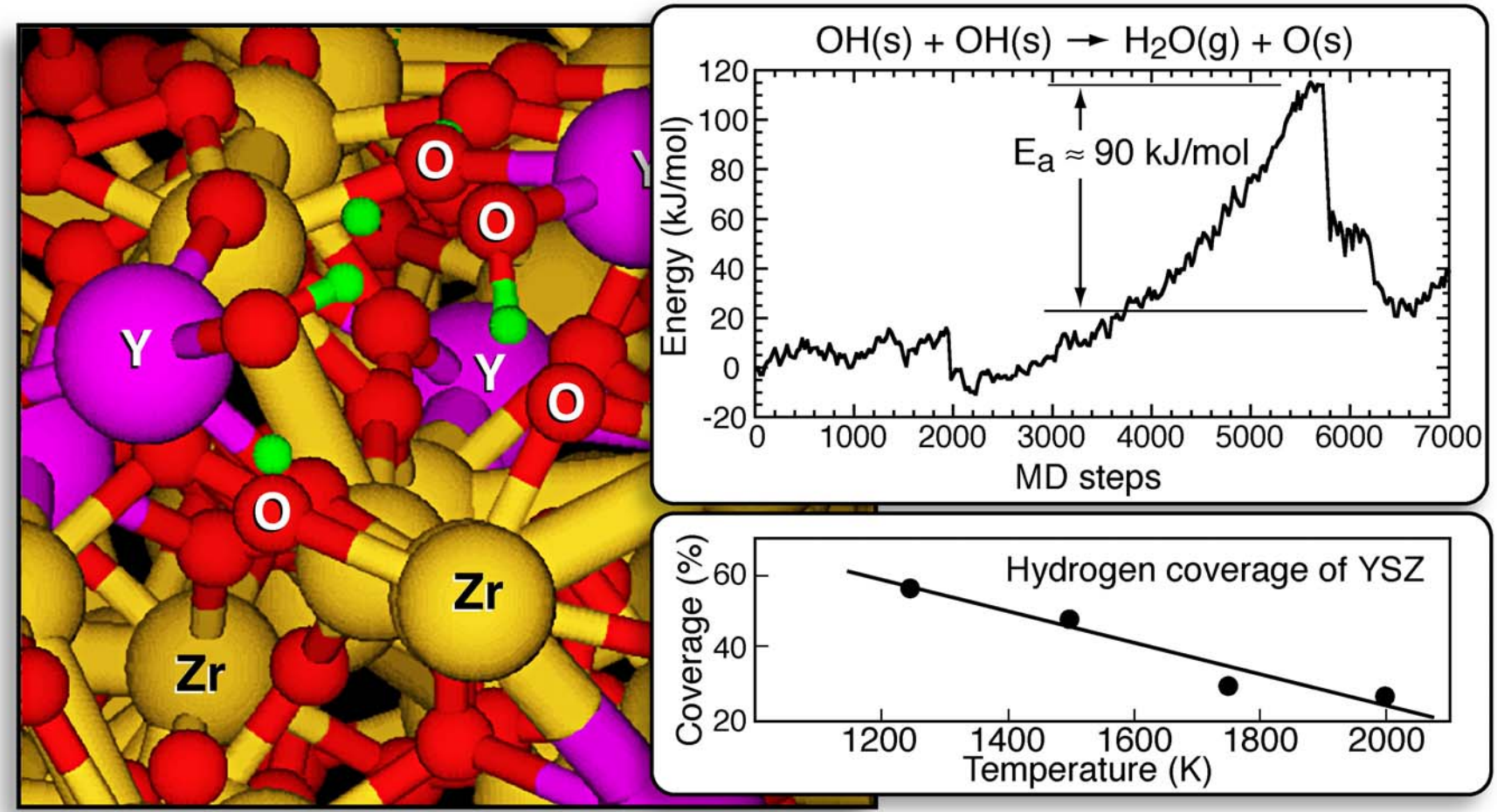

Surface diffusivities are derived from molecular-dynamics simulations

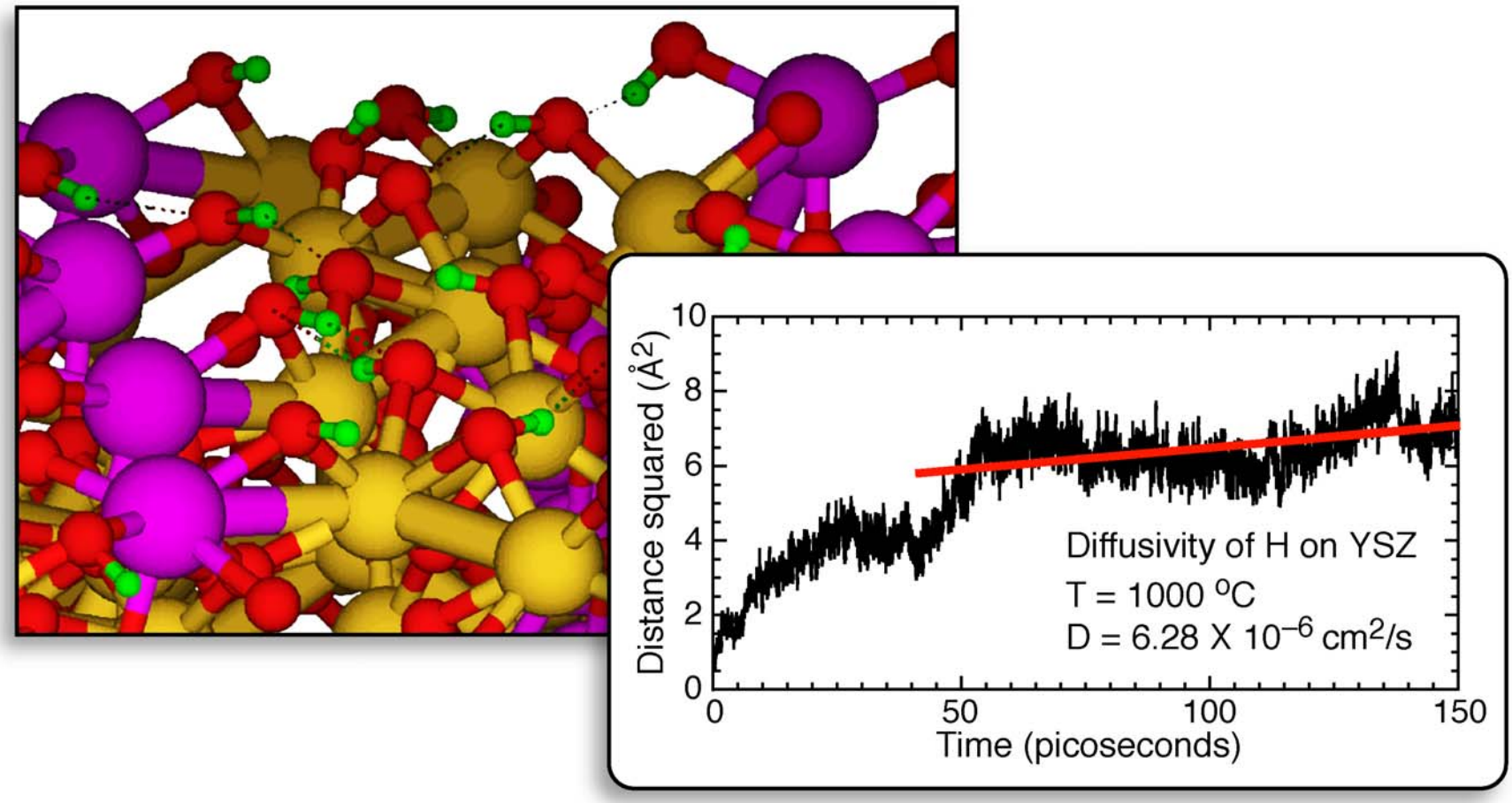

Pattern anodes are an important vehicle to establish the charge-transfer chemistry

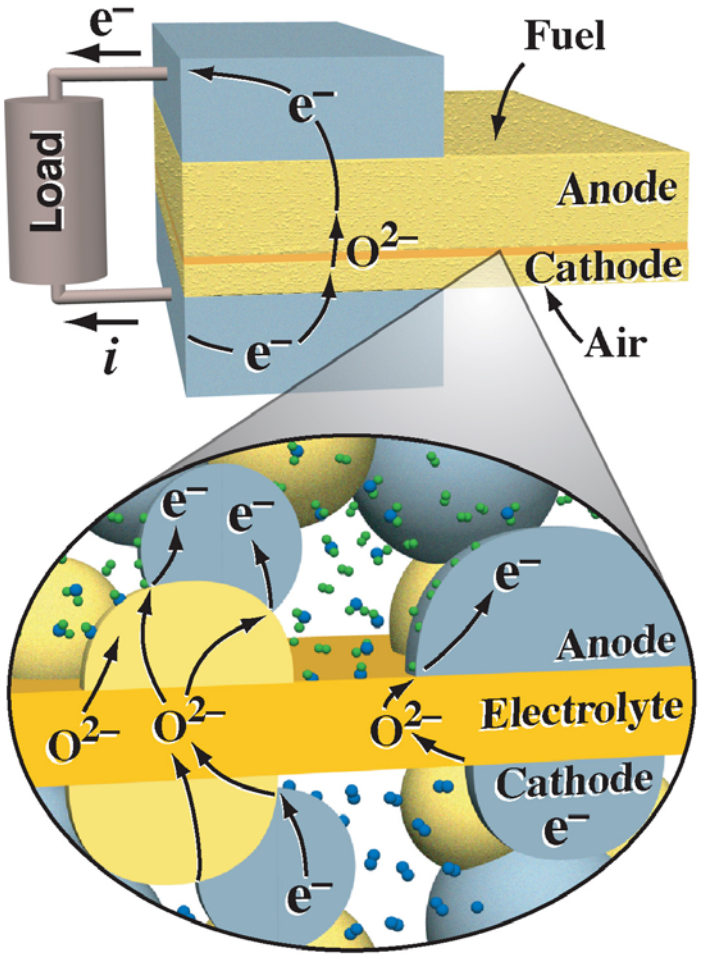

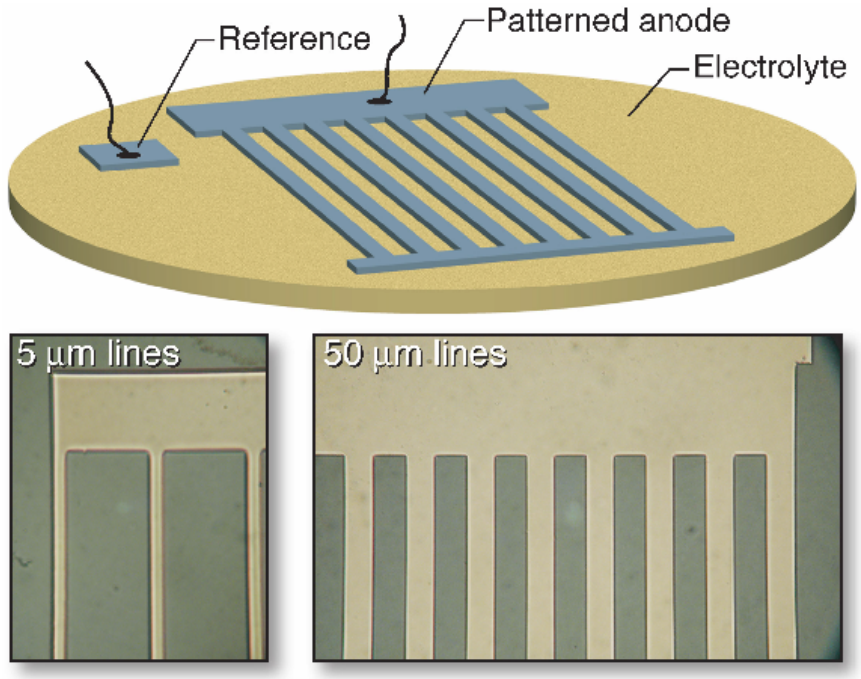

Electrochemical performance
- **Voltage-current characterization**
- **Impedance spectroscopy**

Surface interrogation
- **Micro-Raman spectroscopy**

Pattern anode experiments provide polarization and impedance data

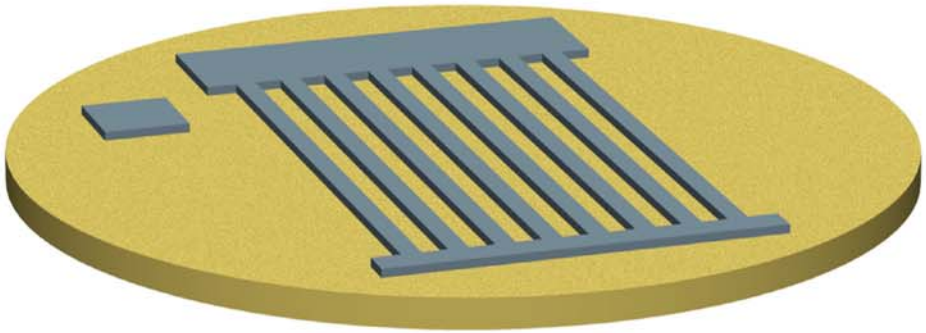

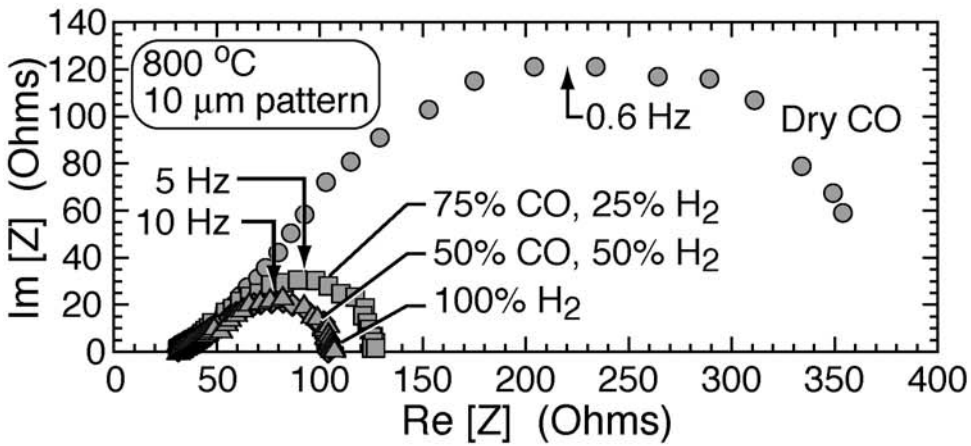

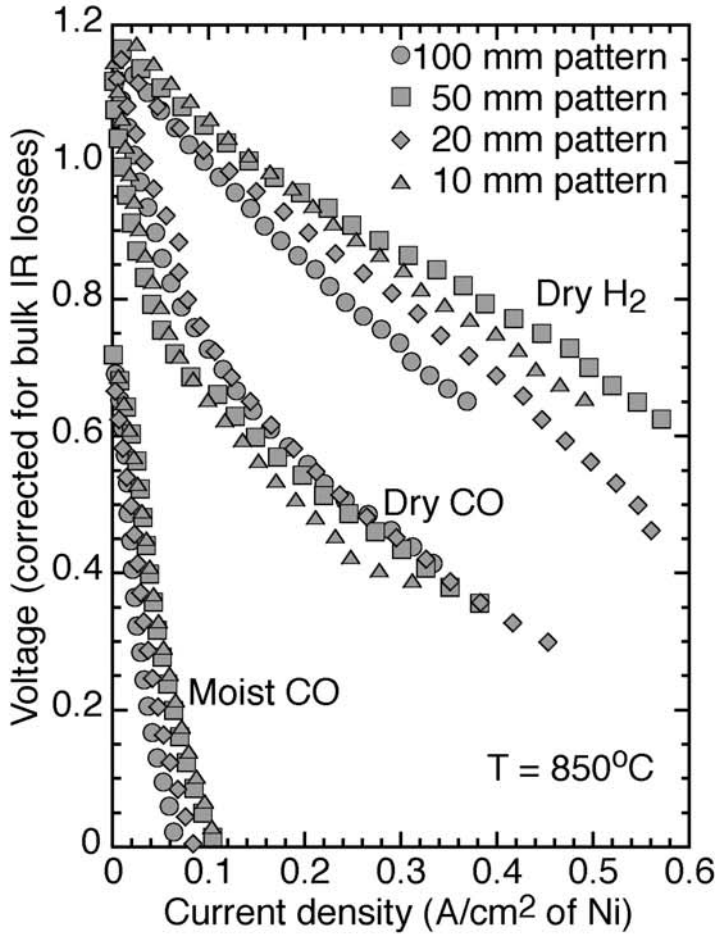

Deposit formation affects pattern-anode cell performance significantly

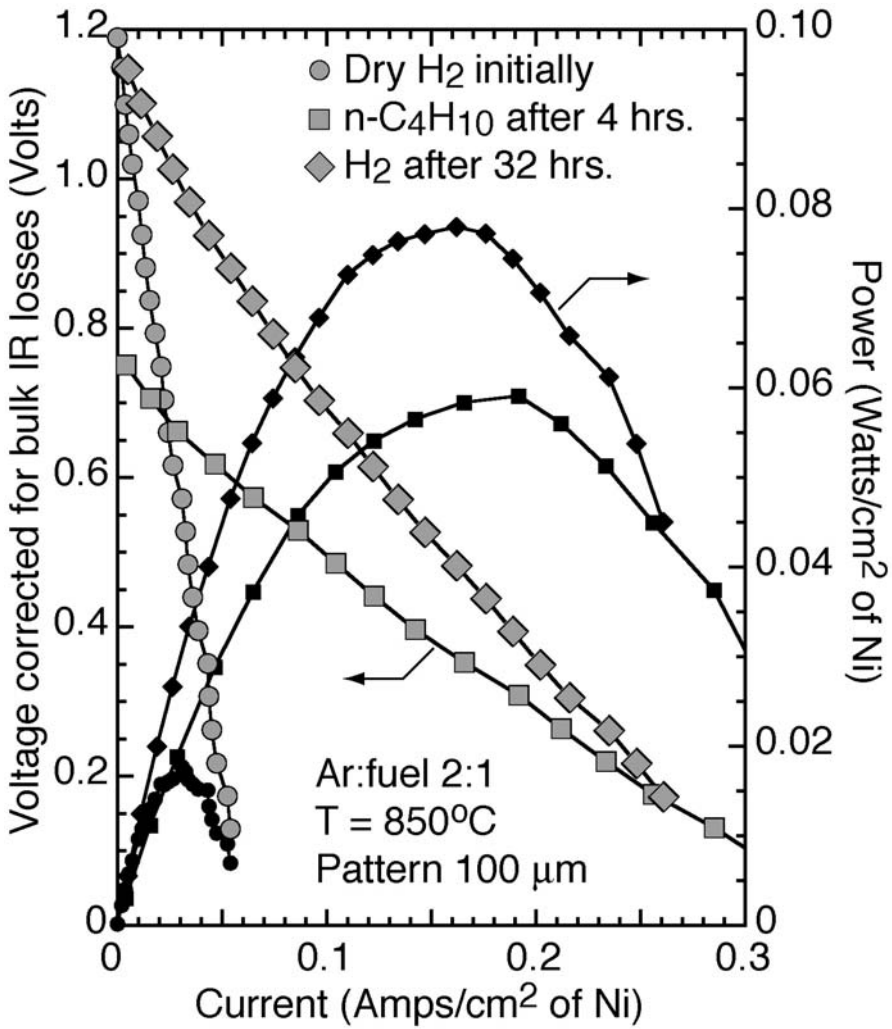

Butane on pattern Ni

- Transient performance
- Surface carbon buildup
- Expands onto electrolyte

Carbon improves performance

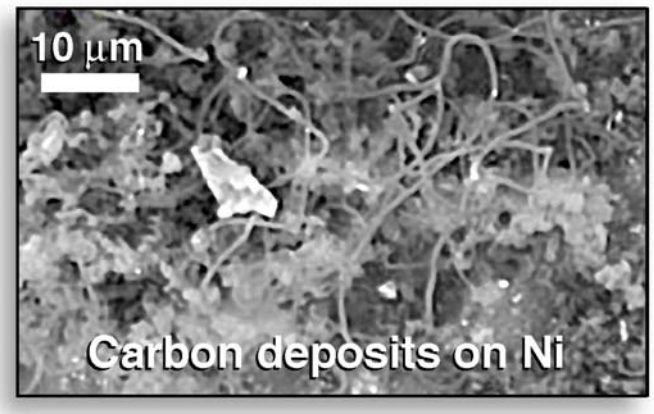

UMCP's optically accessible anode provides a means to interrogate surface chemistry

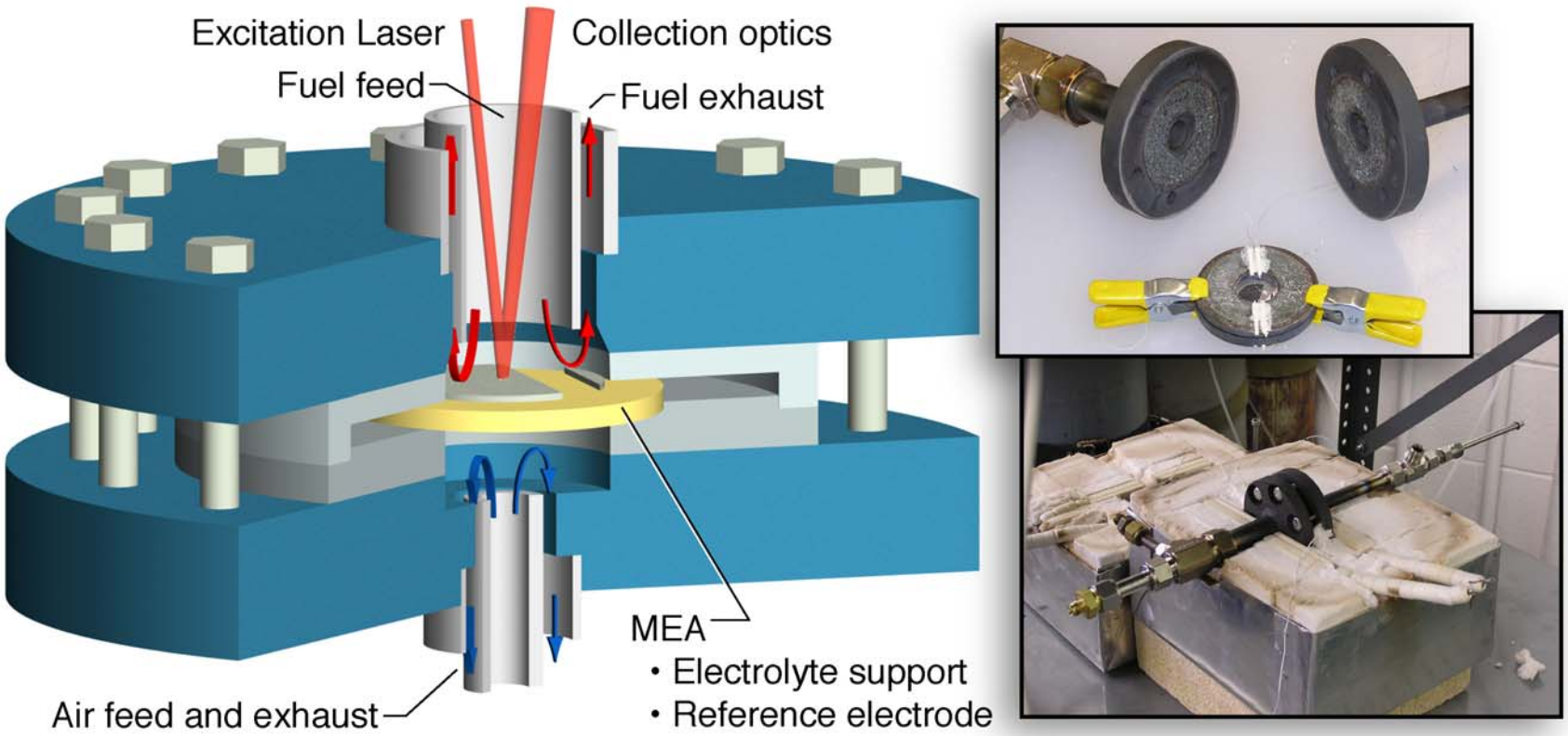

Samaria-doped ceria (SDC15) is characterized with impedance spectroscopy

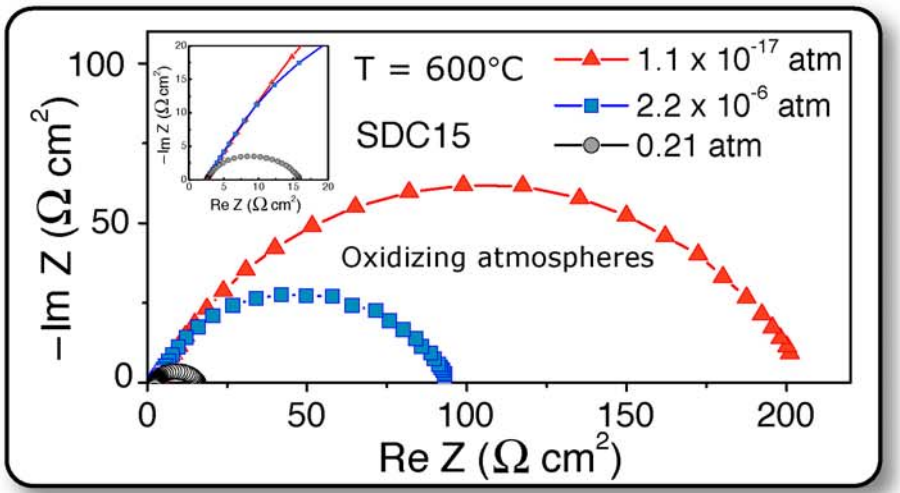

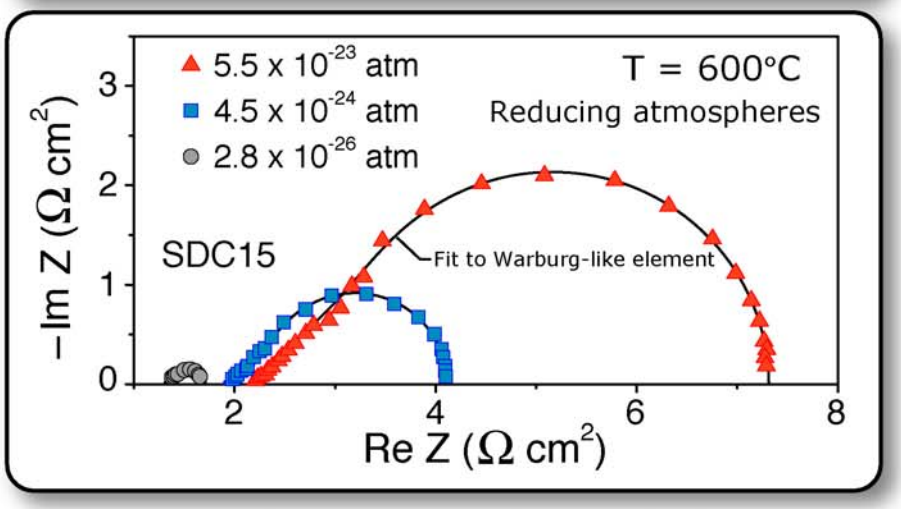

Oxidizing environment: Ar/O_2
Reducing environment: $Ar/H_2/H_2O$

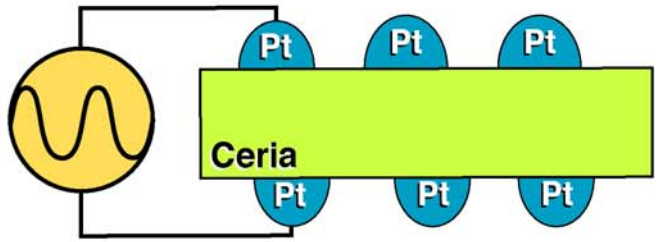

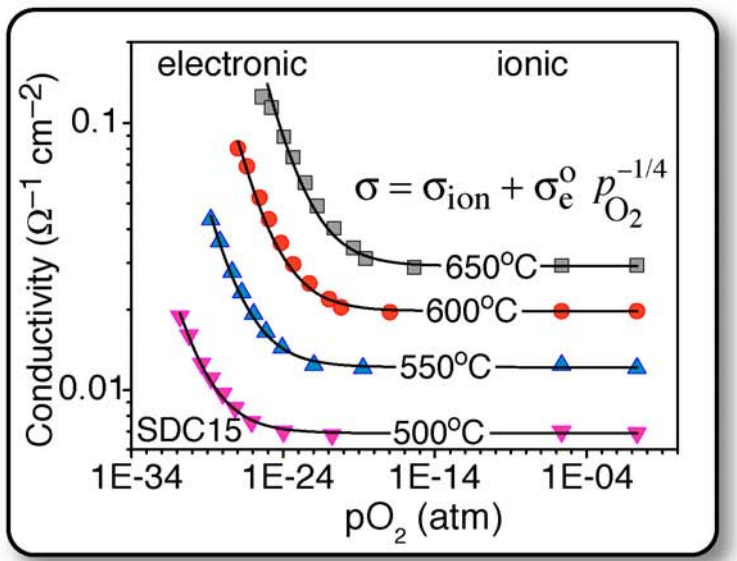

Hydrogen electro-oxidation appears to occur on the ceria surface

$H_2 + O^{=} \rightleftharpoons H_2O + 2e^-$

- Independent of metal
  - Reaction on ceria surface
- Activation energy matches
  - $\sigma_{electronic}$ = 2.31 ± 0.02 eV
- Rate-limiting step
  - electron migration

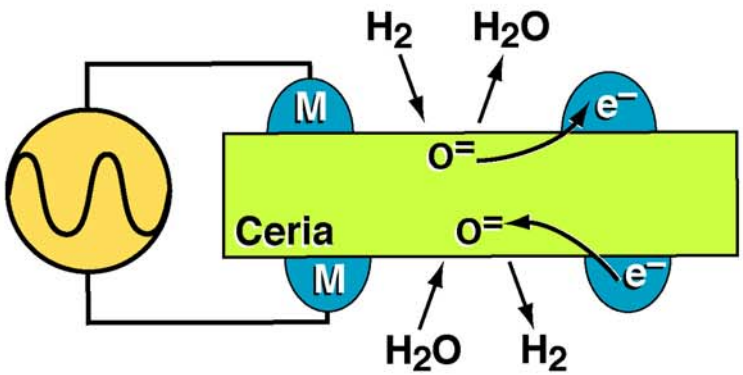

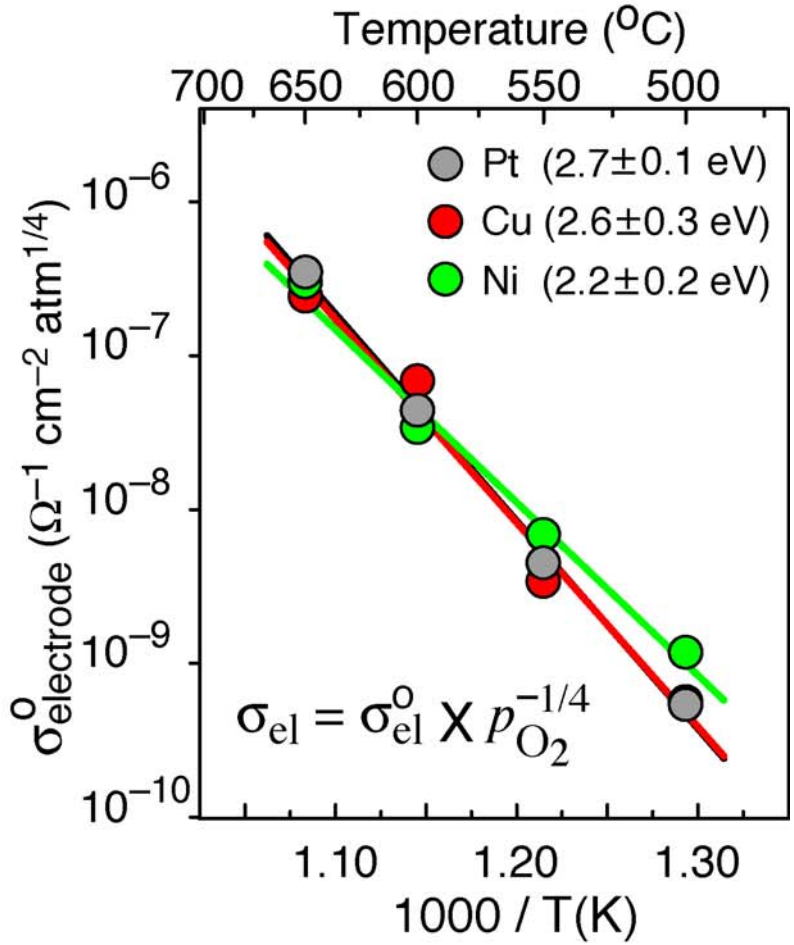

MD simulations reveal the role of different metals in catalyzing carbon growth

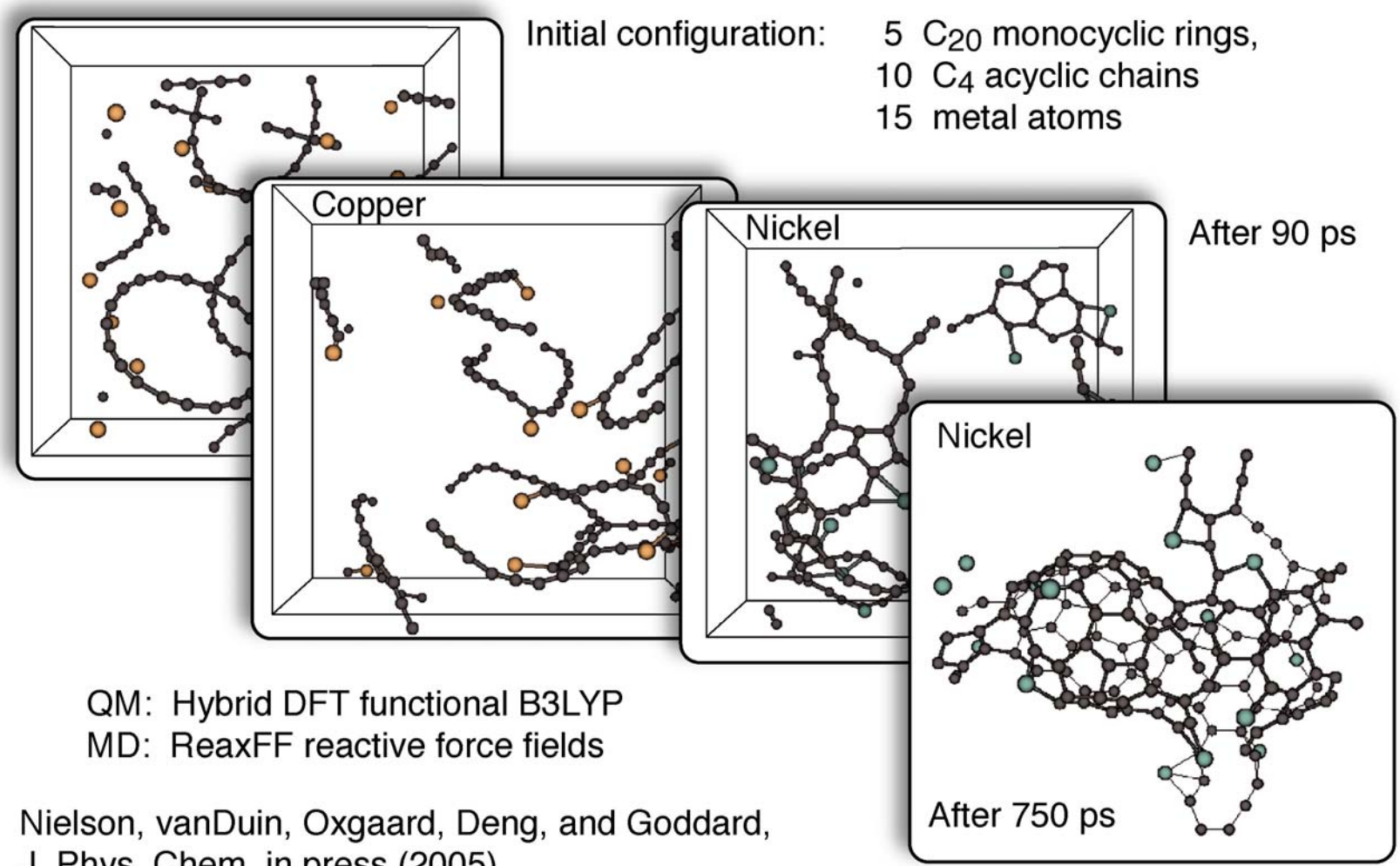

QM: Hybrid DFT functional B3LYP
MD: ReaxFF reactive force fields

Nielson, vanDuin, Oxgaard, Deng, and Goddard,
J. Phys. Chem, in press (2005)

Homogeneous chemistry models predict observed fuel conversion and deposits

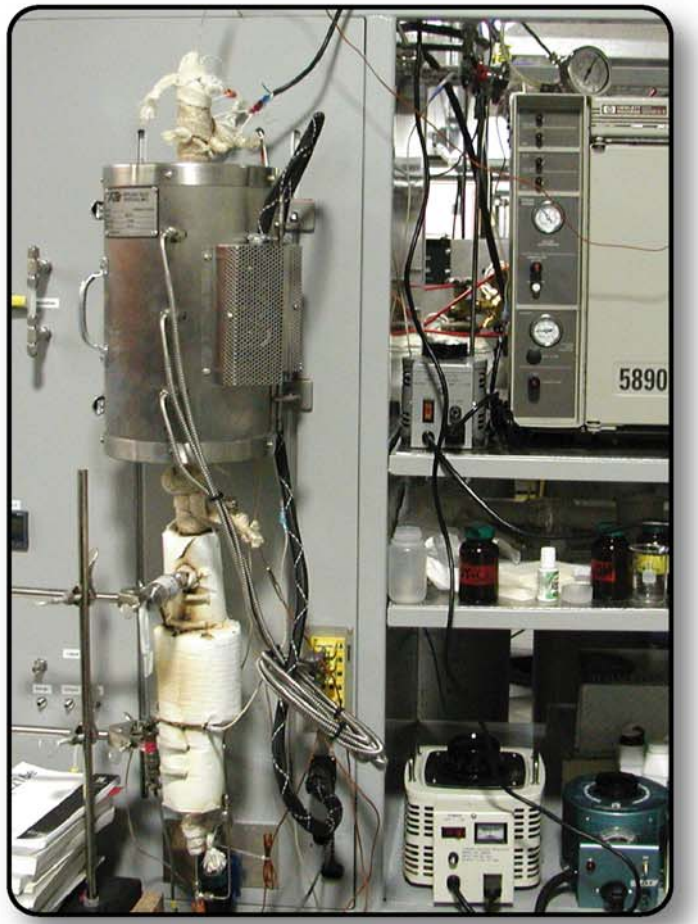

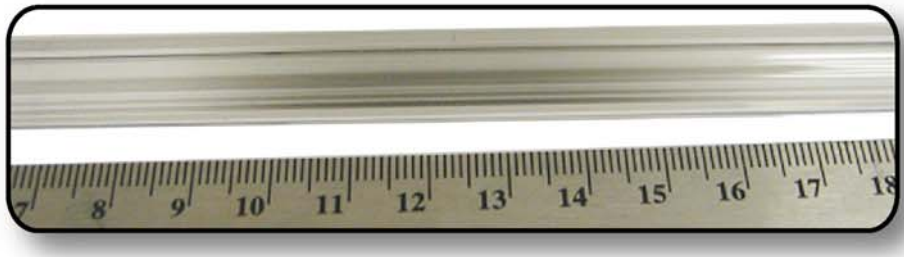

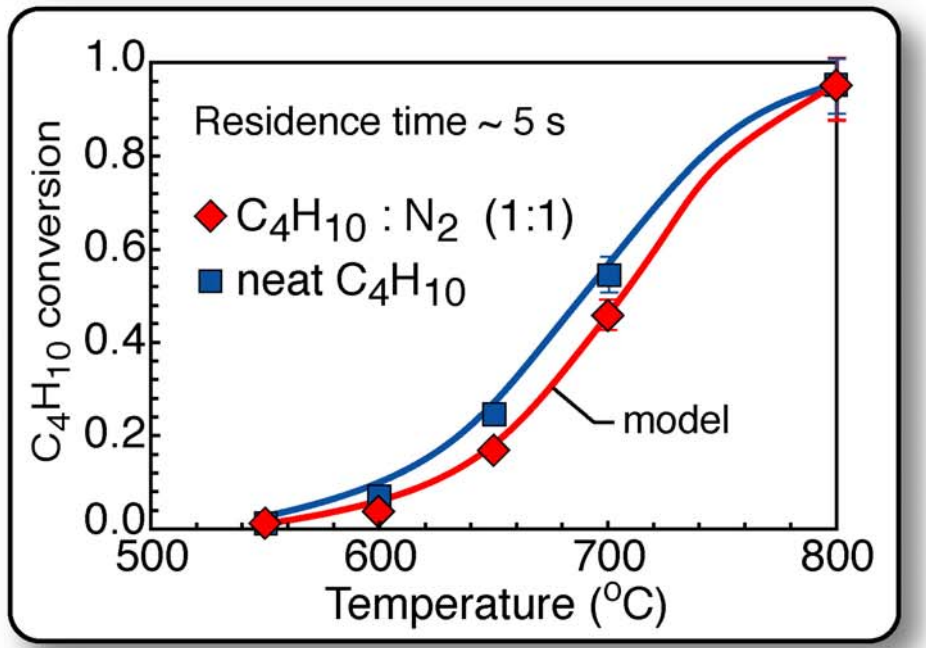

Gas-phase kinetics transforms the fuel as a function of composition and residence time

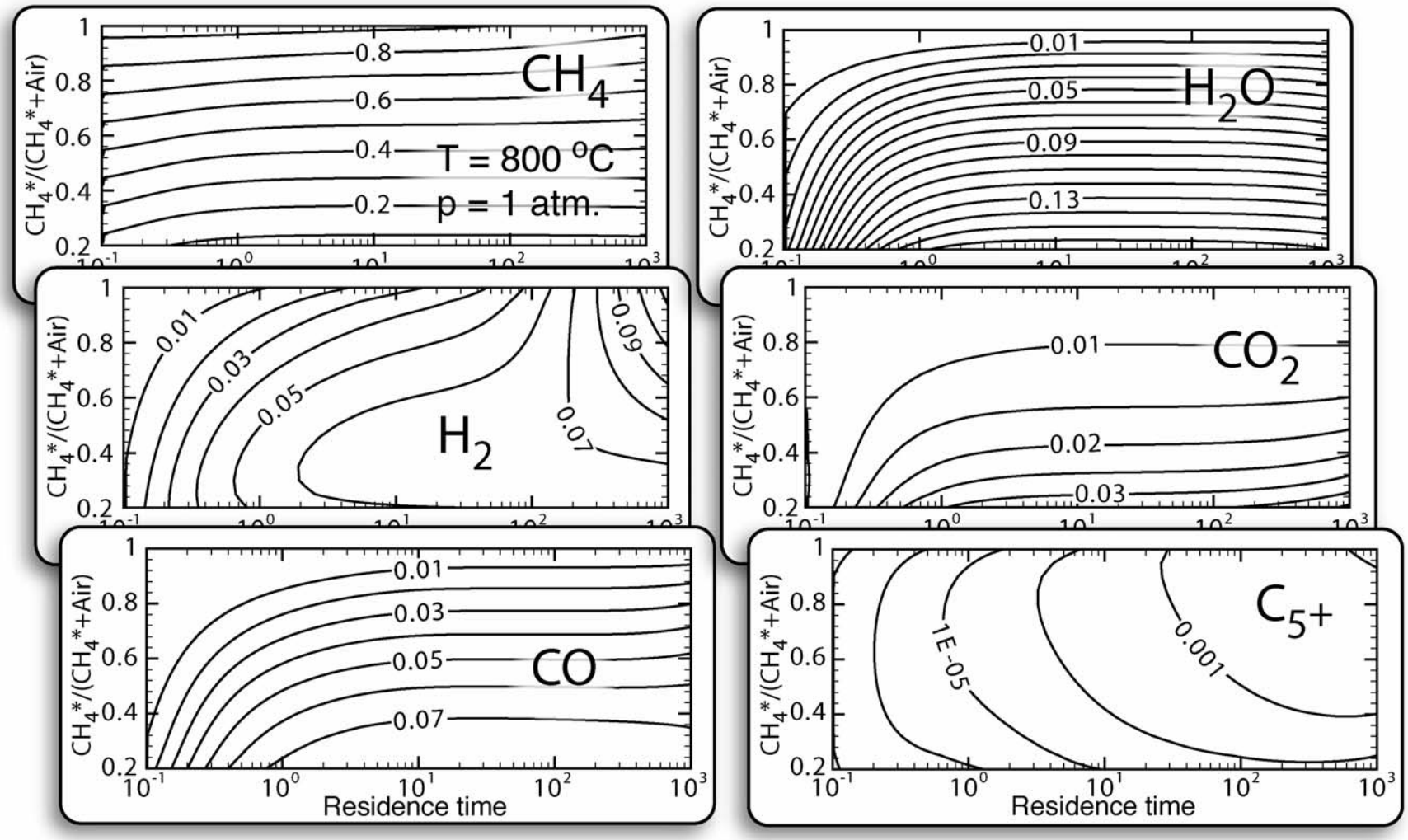

Molecular-weight chemistry is a perturbation on heterogeneous and electrochemistry

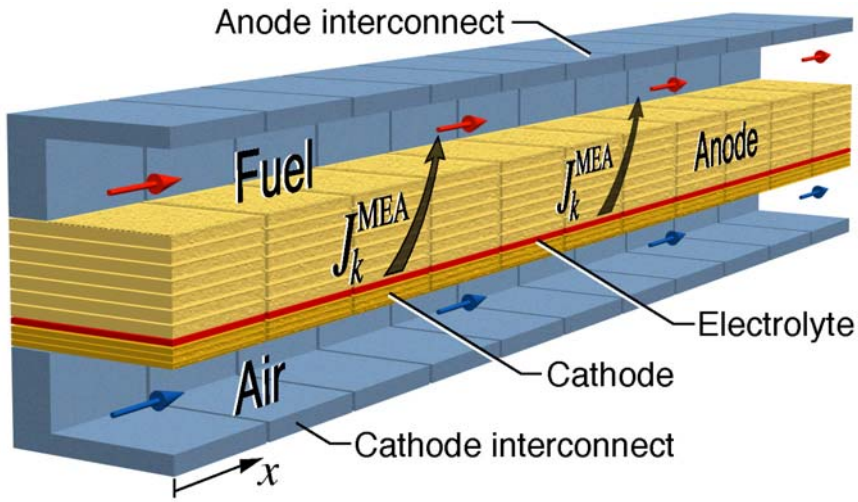

Solve dual-channel model
- Neglect gas-phase chemistry
- Simple gas-phase chemistry
- Include heterogeneous chemistry
- Include electrochemistry

Evaluate fluxes to/from channel

Elementary gas-phase chemistry
- Modified plug flow
- Imposed wall fluxes
- Predict molecular-weight growth

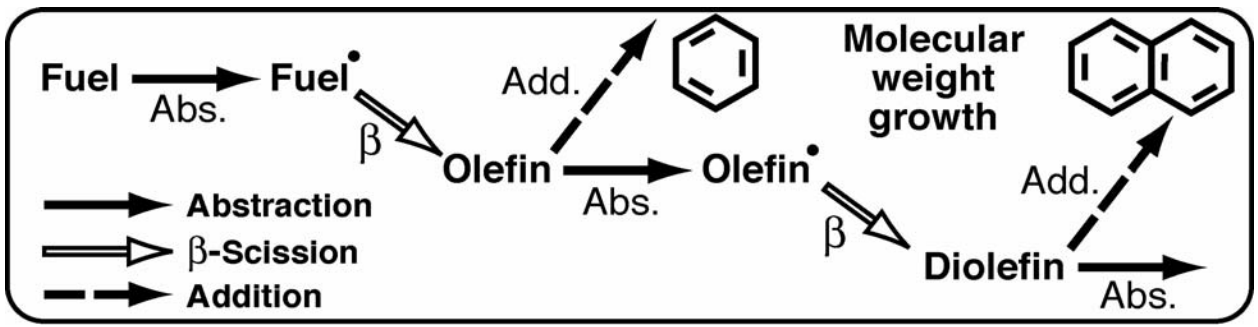

Large mechanism
- ~ 2500 reactions
- ~ 300 species

Combustion
- Soot models

Cell structure and operation affect the gas-phase molecular-weight growth

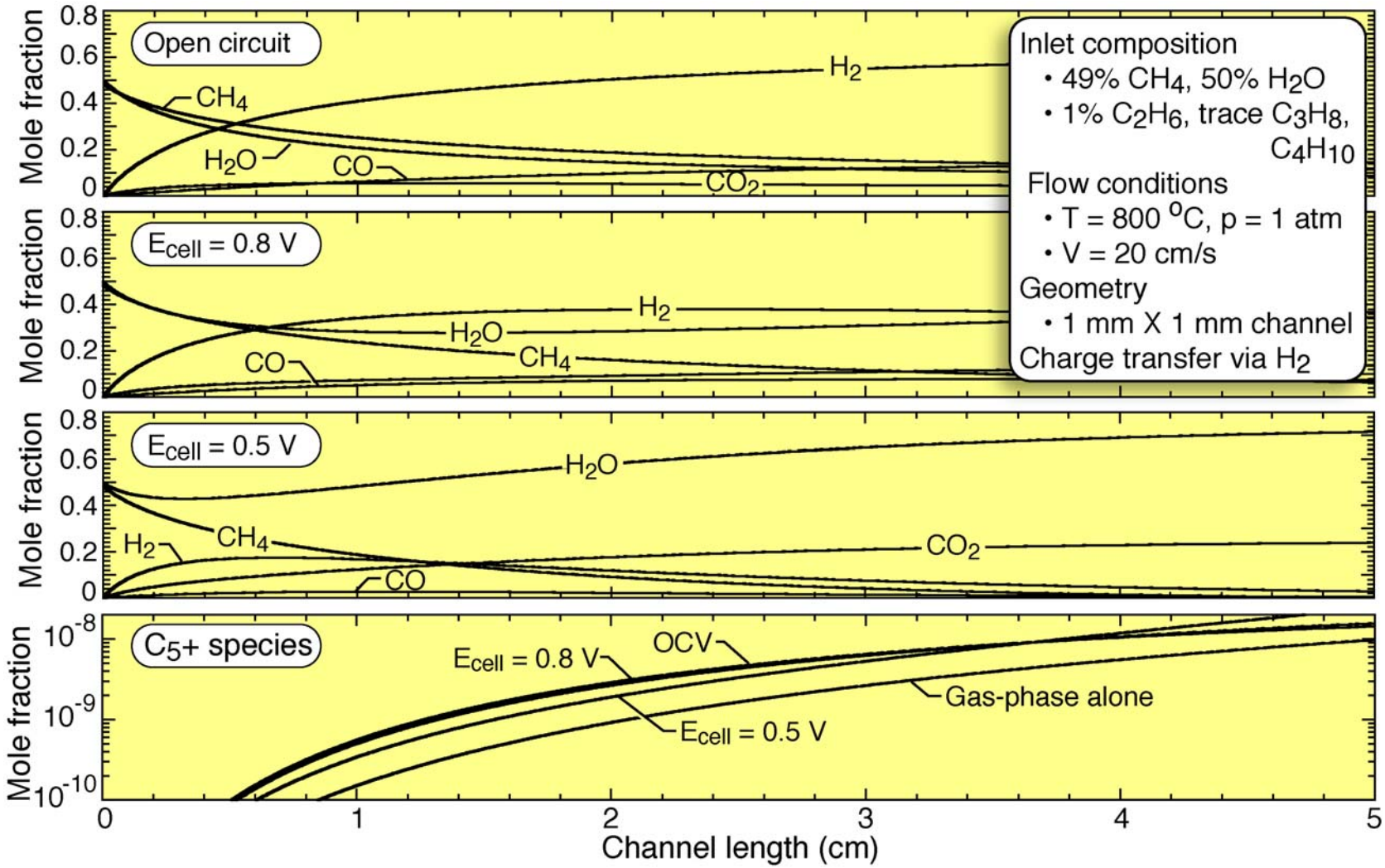

The models incorporate elementary charge-transfer chemistry

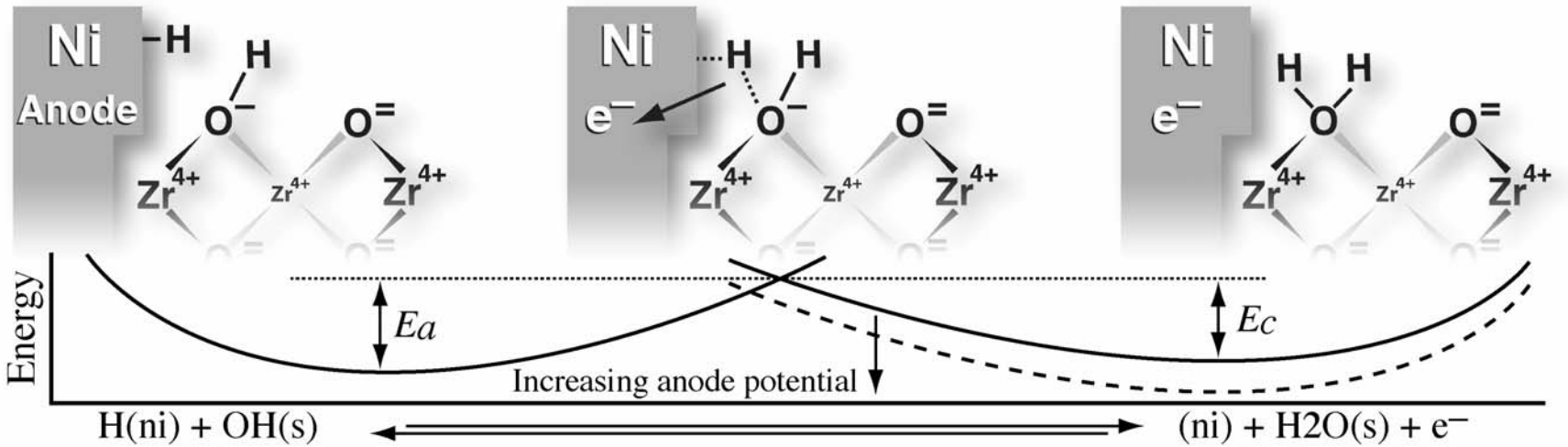

Nickel surface reactions

$H_2 + (ni) + (ni) <=> H(ni) + H(ni)$

$H_2O + (ni) + (ni) <=> OH(ni) + H(ni)$

$OH(ni) + H(ni) <=> O(ni) + H_2 + (ni)$

Triple-phase charge exchange

$H(ni) + O(s) <=> (ni) + e^- + OH(s)$

$H(ni) + OH(s) <=> (ni) + H_2O(s) + e^-$

YSZ surface reactions

$VO(s) + Ox <=> VO + O(s)$

$H_2O(s) <=> H_2O + VO(s)$

Surface and bulk species

(ni)	Empty Ni site
H(ni)	H adsorbed on Ni
OH(ni)	OH adsorbed on Ni
Ox	Bulk oxygen ion, charge = –2
VO	Bulk oxygen vacancy
VO(s)	Oxygen vacancy on YSZ
O(s)	Surface O ion, charge = –2
$H_2O(s)$	Surface H_2O
OH(s)	Surface OH, charge = –1

Goodwin's pattern-anode model is the first of its kind

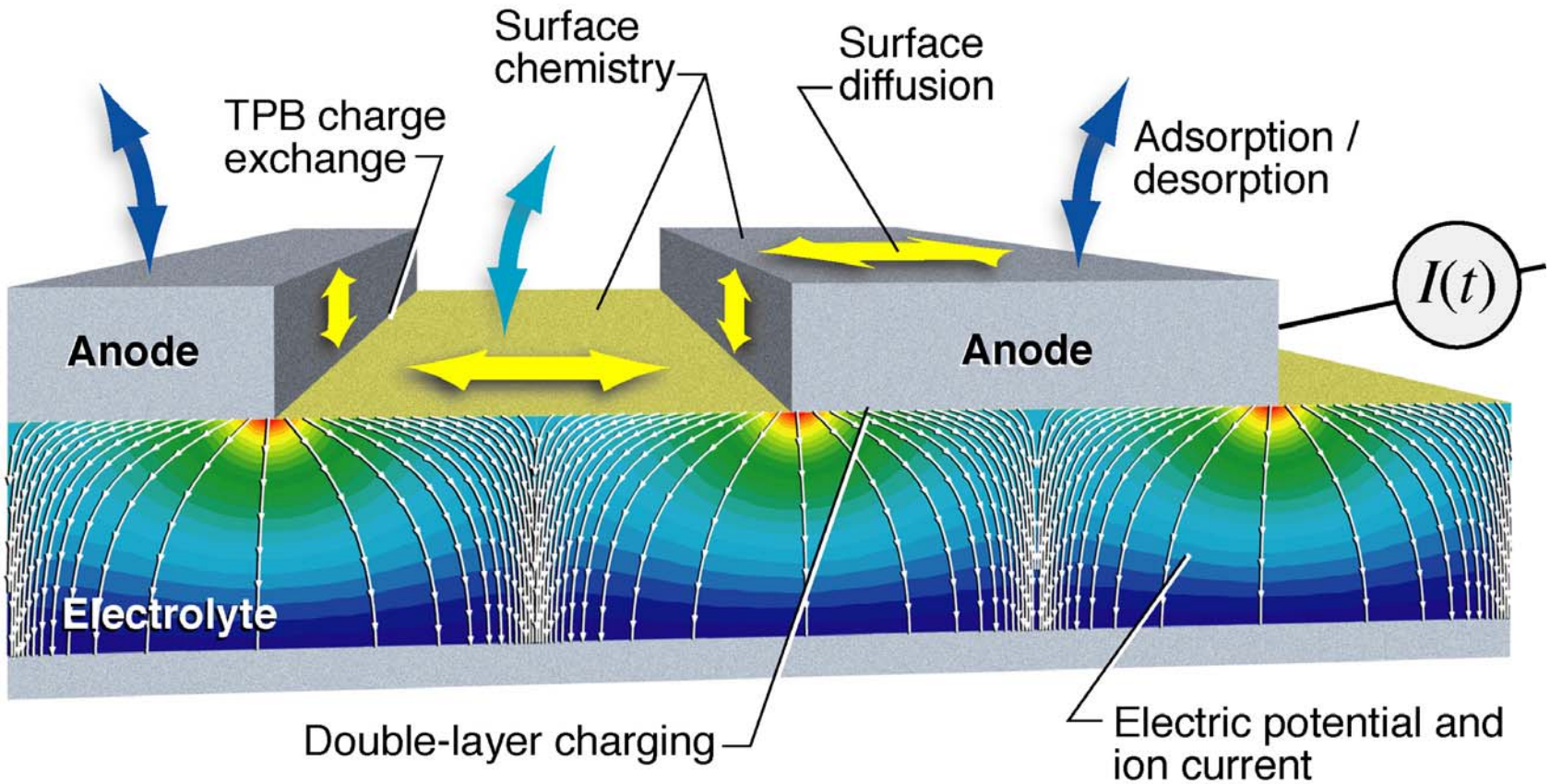

Performance is predicted from elementary chemistry and thermodynamics

Reaction	A	E
$H_2(g)+2(Ni) \rightleftharpoons 2H(Ni)$,	0.4[a]	0
$H(Ni)+O''_{ad} \rightleftharpoons (Ni)+OH'_{ad}+e'$	5×10^{16}	90
$H(Ni)+OH'_{ad} \rightleftharpoons (Ni)+H_2O_{ad}+e'$	5×10^{15}	90
$H_2O(g)+(s) \rightleftharpoons H_2O_{ad}$	1.0[a]	0
$O_x+(s) \rightleftharpoons V_O^{\cdot\cdot}+O''_{ad}$	5×10^{8}	0

Species	h^0 (kJ/mol)	s^0 (J/mol/K)
$H_2(g)$	24.4	169.8
$H_2O(g)$	-210.6	237.6
(Ni)	0	0
$H(Ni)$	-35.81	36.77
O''_{ad}	-170.0	50.0
OH''_{ad}	-220.0	87.0
H_2O_{ad}	-265.0	98.1
O_x	-170.0	50.0
$V_O^{\cdot\cdot}$	0	0
(s)	0	0

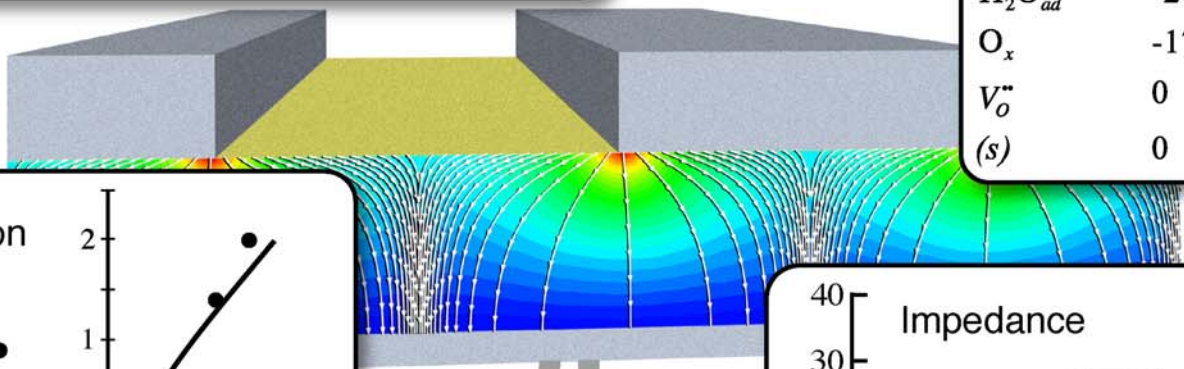

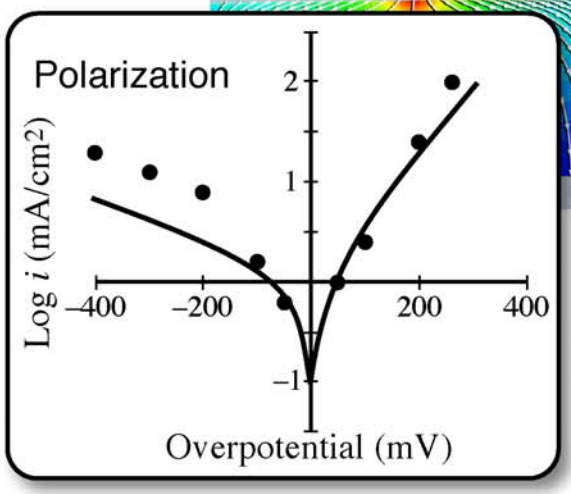

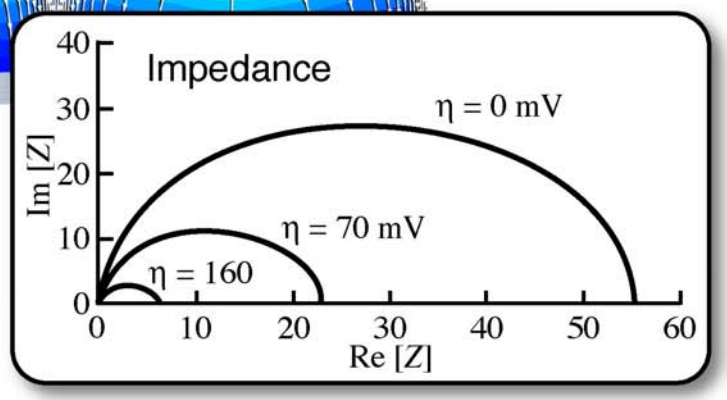

What is the role of the anode structure in promoting reforming, shifting, and CPOX

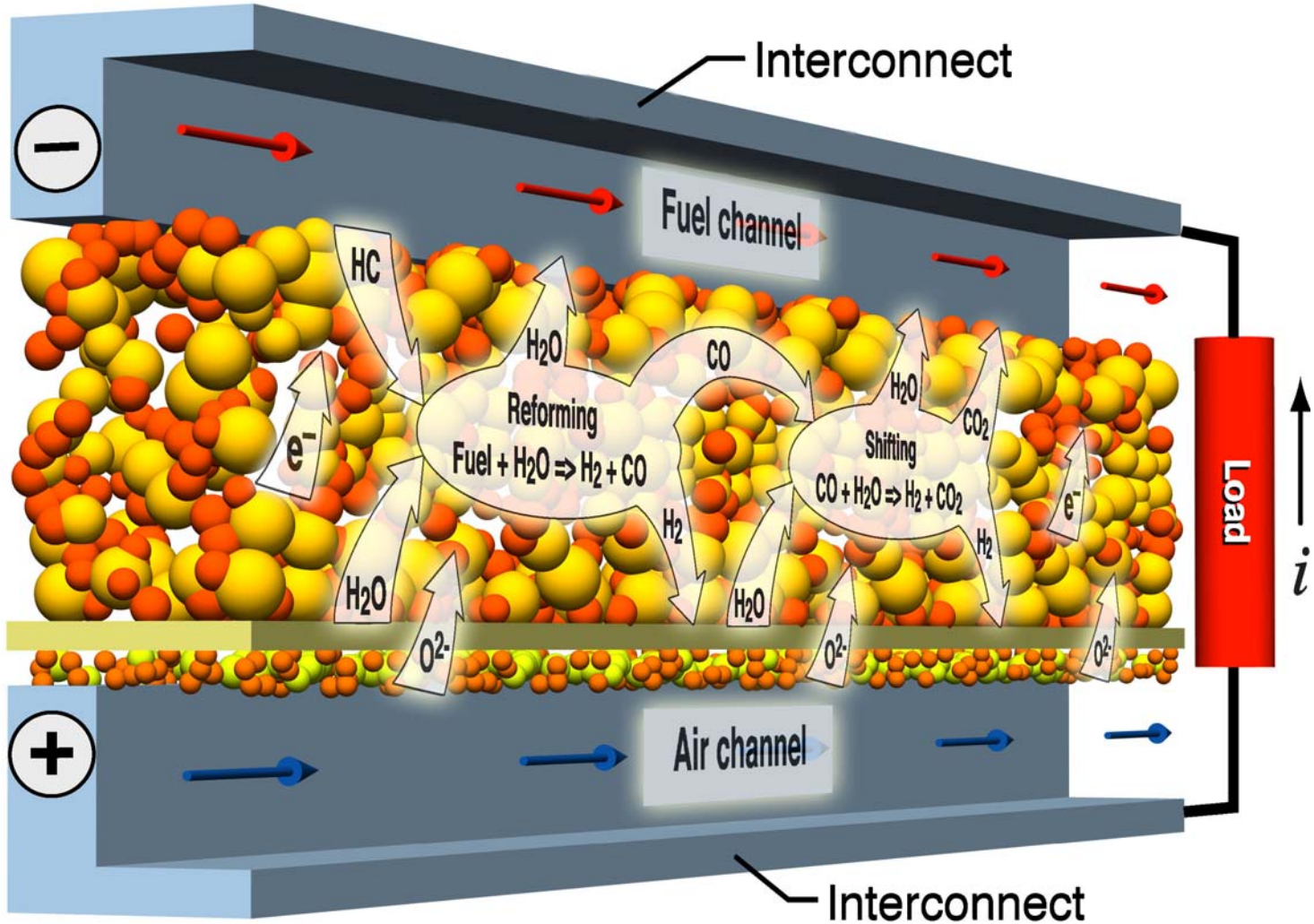

MEA models do a good job of representing measured electrochemical performance

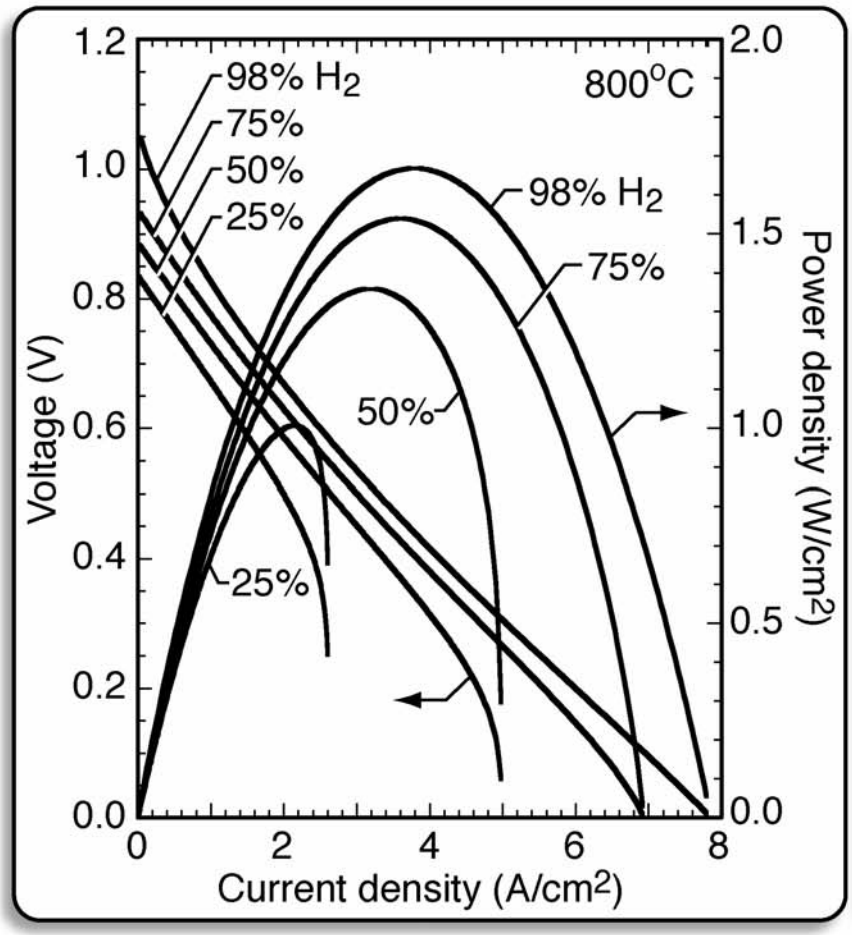

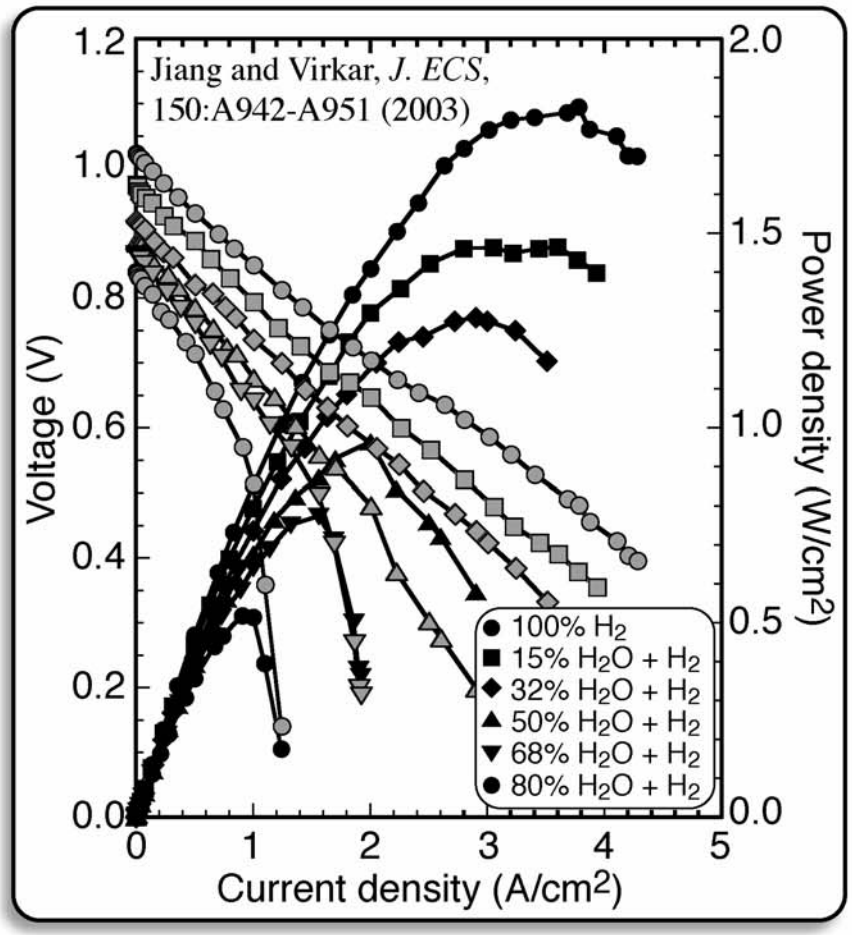

The Dusty-Gas model applies when the mean-free path is comparable to the pore size

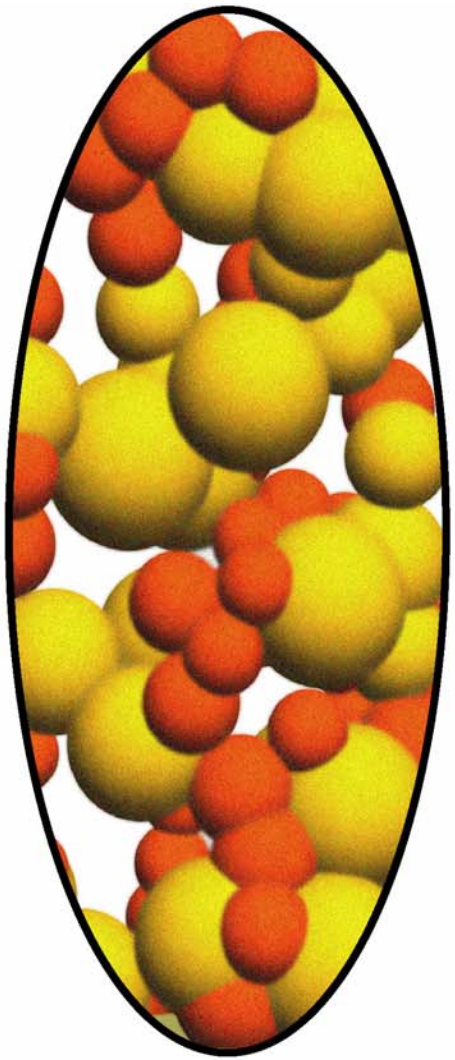

Dusty-gas model

$$\sum_{\ell \neq k} \frac{[X_\ell]\mathbf{J}_k - [X_k]\mathbf{J}_\ell}{[X_T]D^{\mathrm{e}}_{k\ell}} + \frac{\mathbf{J}_k}{D^{\mathrm{e}}_{k,\mathrm{Kn}}} = -\nabla[X_k] - \frac{[X_k]}{D^{\mathrm{e}}_{k,\mathrm{Kn}}}\frac{B_{\mathrm{g}}}{\mu}\nabla p$$

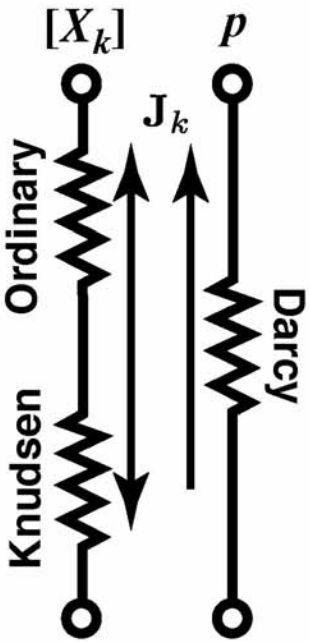

Effective Binary and Knudsen diffusion

$$D^{\mathrm{e}}_{k\ell} = \frac{\phi_{\mathrm{g}}}{\tau_{\mathrm{g}}} D_{k\ell} \qquad D^{\mathrm{e}}_{k,\mathrm{Kn}} = \frac{4}{3}\frac{r_p \phi_{\mathrm{g}}}{\tau_{\mathrm{g}}}\sqrt{\frac{8RT}{\pi W_k}}$$

Permeability (Kozeny-Carman)

$$B_{\mathrm{g}} = \frac{\phi_{\mathrm{g}}^3 d_p^2}{72\tau_{\mathrm{g}}\left(1-\phi_{\mathrm{g}}\right)^2}$$

$\mathbf{J}_k$	Molar flux	ϕ_{g}	Porosity
$[X_k]$	Concentration	τ_{g}	Tortuosity
p	Pressure	r_p	Pore radius
		d_p	Particle diameter

The models accommodate elementary heterogeneous reforming/CPOX chemistry

	Reaction	A^*	E_a^*
Adsorption:			
1.	$H_2 + Ni(s) + Ni(s) \rightarrow H(s) + H(s)$	$1.000 \cdot 10^{-2\dagger}$	0.0
2.	$O_2 + Ni(s) + Ni(s) \rightarrow O(s) + O(s)$	$1.000 \cdot 10^{-2\dagger}$	0.0
3.	$CH_4 + Ni(s) \rightarrow CH_4(s)$	$8.000 \cdot 10^{-3\dagger}$	0.0
4.	$H_2O + Ni(s) \rightarrow H_2O(s)$	$1.000 \cdot 10^{-1\dagger}$	0.0
5.	$CO_2 + Ni(s) \rightarrow CO_2(s)$	$1.000 \cdot 10^{-5\dagger}$	0.0
Desorption:			
6.	$CO + Ni(s) \rightarrow CO(s)$	$5.000 \cdot 10^{-1\dagger}$	0.0
7.	$H(s) + H(s) \rightarrow Ni(s) + Ni(s) + H_2$	$3.000 \cdot 10^{21}$	98.0
8.	$O(s) + O(s) \rightarrow Ni(s) + Ni(s) + O_2$	$1.300 \cdot 10^{22}$	464.0
9.	$H_2O(s) \rightarrow H_2O + Ni(s)$	$6.000 \cdot 10^{13}$	68.9
10.	$CO(s) \rightarrow CO + Ni(s)$	$1.000 \cdot 10^{13}$	122.4
		$\theta_{CO(s)}$	-50.0
11.	$CO_2(s) \rightarrow CO_2 + Ni(s)$	$1.000 \cdot 10^{8}$	27.3
12.	$CH_4(s) \rightarrow CH_4 + Ni(s)$	$2.000 \cdot 10^{14}$	25.1
13.	$H(s) + O(s) \rightarrow OH(s) + Ni(s)$	$5.000 \cdot 10^{22}$	97.9
Surface reaction:			
14.	$OH(s) + Ni(s) \rightarrow H(s) + O(s)$	$3.000 \cdot 10^{20}$	34.3
15.	$H(s) + OH(s) \rightarrow H_2O(s) + Ni(s)$	$3.000 \cdot 10^{20}$	42.7
16.	$H_2O(s) + Ni(s) \rightarrow H(s) + OH(s)$	$3.000 \cdot 10^{22}$	87.0
17.	$OH(s) + OH(s) \rightarrow H_2O(s) + O(s)$	$3.000 \cdot 10^{21}$	100.0
18.	$H_2O(s) + O(s) \rightarrow OH(s) + OH(s)$	$3.000 \cdot 10^{21}$	207.5
19.	$C(s) + O(s) \rightarrow CO(s) + Ni(s)$	$5.200 \cdot 10^{23}$	148.1
20.	$CO(s) + Ni(s) \rightarrow C(s) + O(s)$	$2.500 \cdot 10^{21}$	139.7
		$\theta_{CO(s)}$	-50.0
21.	$CO(s) + O(s) \rightarrow CO_2(s) + Ni(s)$	$2.000 \cdot 10^{20}$	123.6
	$(s) \rightarrow CO(s) + O(s)$	$3.000 \cdot 10^{23}$	88.0
	$(s) \rightarrow CH_3(s) + H(s)$	$3.700 \cdot 10^{21}$	57.7
	$(s) \rightarrow CH_4(s) + Ni(s)$	$3.700 \cdot 10^{21}$	56.1
	$(s) \rightarrow CH_2(s) + H(s)$	$3.700 \cdot 10^{24}$	100.0
	$(s) \rightarrow CH_3(s) + Ni(s)$	$3.700 \cdot 10^{21}$	49.8
	$(s) \rightarrow CH(s) + H(s)$	$3.700 \cdot 10^{24}$	97.1
	$) \rightarrow CH_2(s) + Ni(s)$	$3.700 \cdot 10^{24}$	73.6
	$s) \rightarrow C(s) + H(s)$	$3.700 \cdot 10^{21}$	18.8
	$\rightarrow CH(s) + Ni(s)$	$3.700 \cdot 10^{21}$	173.6
	$(s) \rightarrow CH_3(s) + OH(s)$	$1.700 \cdot 10^{24}$	88.3
	$H(s) \rightarrow CH_4(s) + O(s)$	$3.700 \cdot 10^{21}$	23.4
	$(s) \rightarrow CH_2(s) + OH(s)$	$3.700 \cdot 10^{24}$	130.1
	$H(s) \rightarrow CH_3(s) + O(s)$	$3.700 \cdot 10^{21}$	16.7
	$(s) \rightarrow CH(s) + OH(s)$	$3.700 \cdot 10^{24}$	126.8
	$(s) \rightarrow CH_2(s) + O(s)$	$3.700 \cdot 10^{21}$	40.2
	$) \rightarrow C(s) + OH(s)$	$3.700 \cdot 10^{21}$	48.1
	$) \rightarrow CH(s) + O(s)$	$3.700 \cdot 10^{21}$	139.7
	$) \rightarrow HCO(s) + Ni(s)$	$5.000 \cdot 10^{19}$	96.2
	$i(s) \rightarrow CO(s) + H(s)$	$3.700 \cdot 10^{21}$	0.0
		$\theta_{CO(s)}$	50.0
	$i(s) \rightarrow CH(s) + O(s)$	$3.700 \cdot 10^{24}$	95.8
	$) \rightarrow HCO(s) + Ni(s)$	$3.700 \cdot 10^{21}$	146.0

ers for the rate constants written in the form:
$_a/RT)$. The units of A are given in terms of moles,
conds. E_a is in kJ/mol.
ions 20 and 41, -0.97 for reactions 22 and 39.
t.
ge (e.g., $\theta_{CO(s)}$) is specified as a site fraction.
ace site density is $\Gamma = 2.60 \times 10^{-9}$ mol/cm^2.

Collaboration with Olaf Deutschmann, University of Karlsruhe

The separated-anode experiment is designed to isolate thermal heterogeneous chemistry

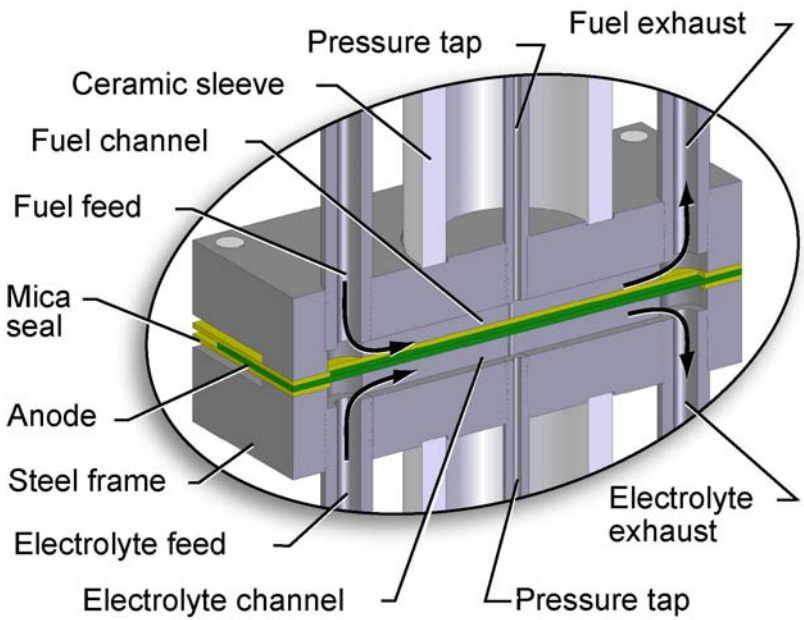

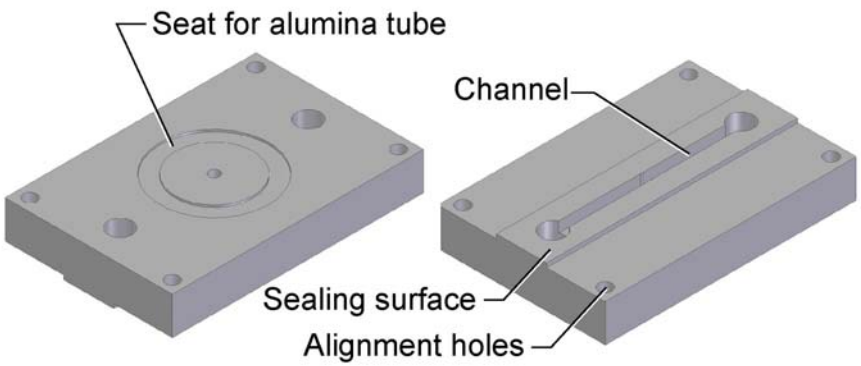

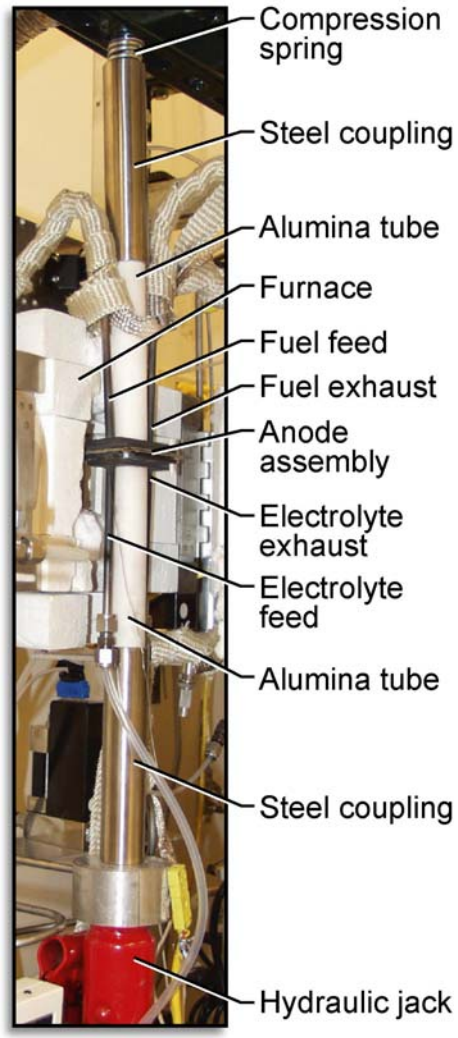

Dry reforming (CO_2) is nearly as effective as steam reforming

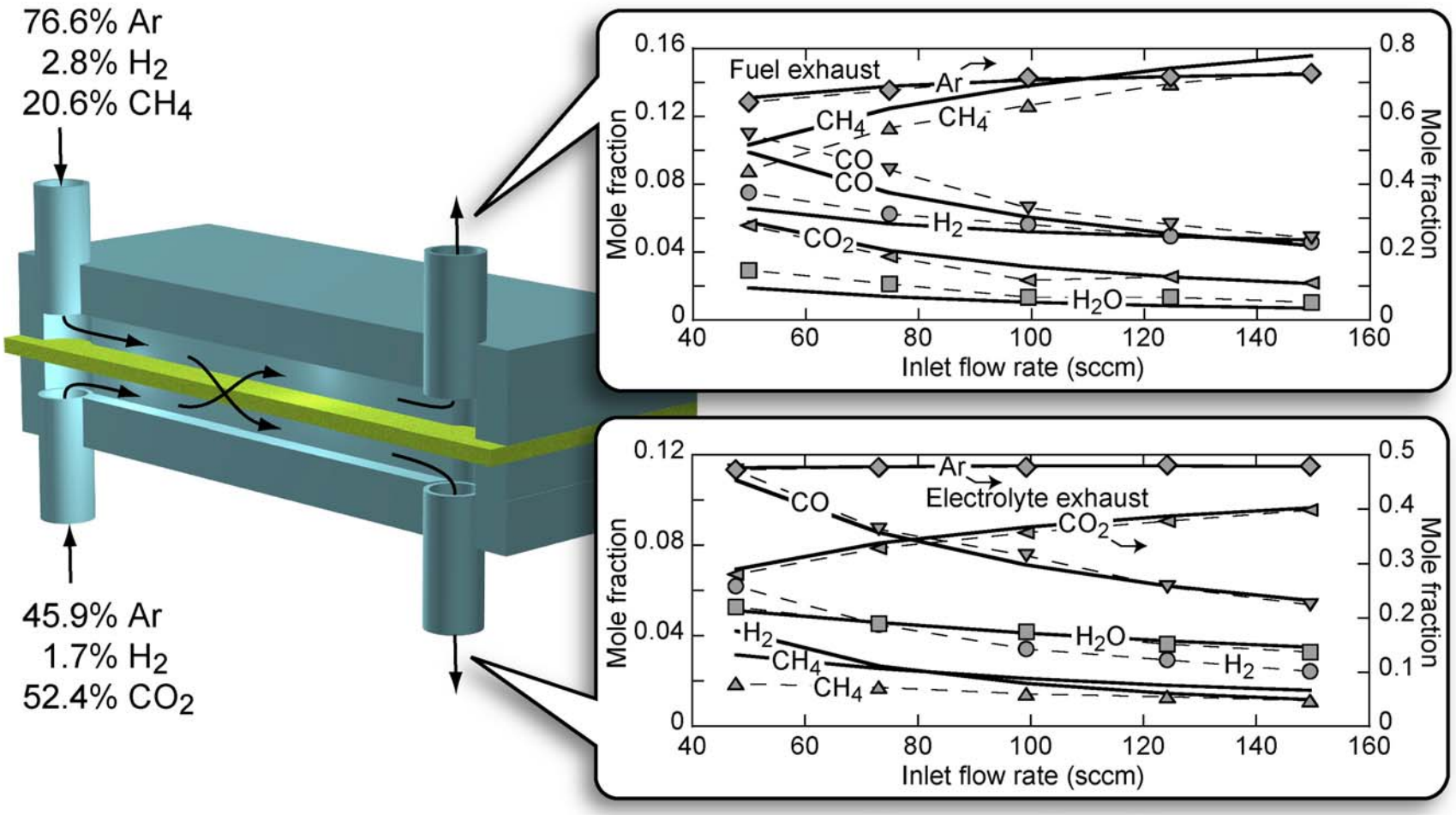

Our models incorporate coupled fluid flow, thermal chemistry, and electrochemistry

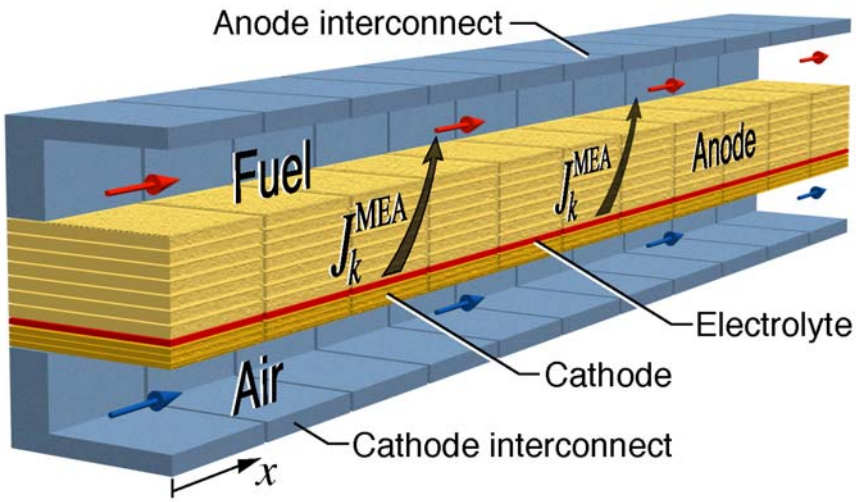

Approach
- Reactive flow
- Porous-media transport
- Homogeneous chemistry
- Heterogeneous chemistry
- Electrochemistry

Design
- MEA architecture
- Catalyst materials
- Electrode microstructure

Operation
- Cell voltage
- Flow rates
- Fuel mixtures

Performance
- Efficiency
- Utilization
- Power density

The models predict composition along the channels and through the electrodes

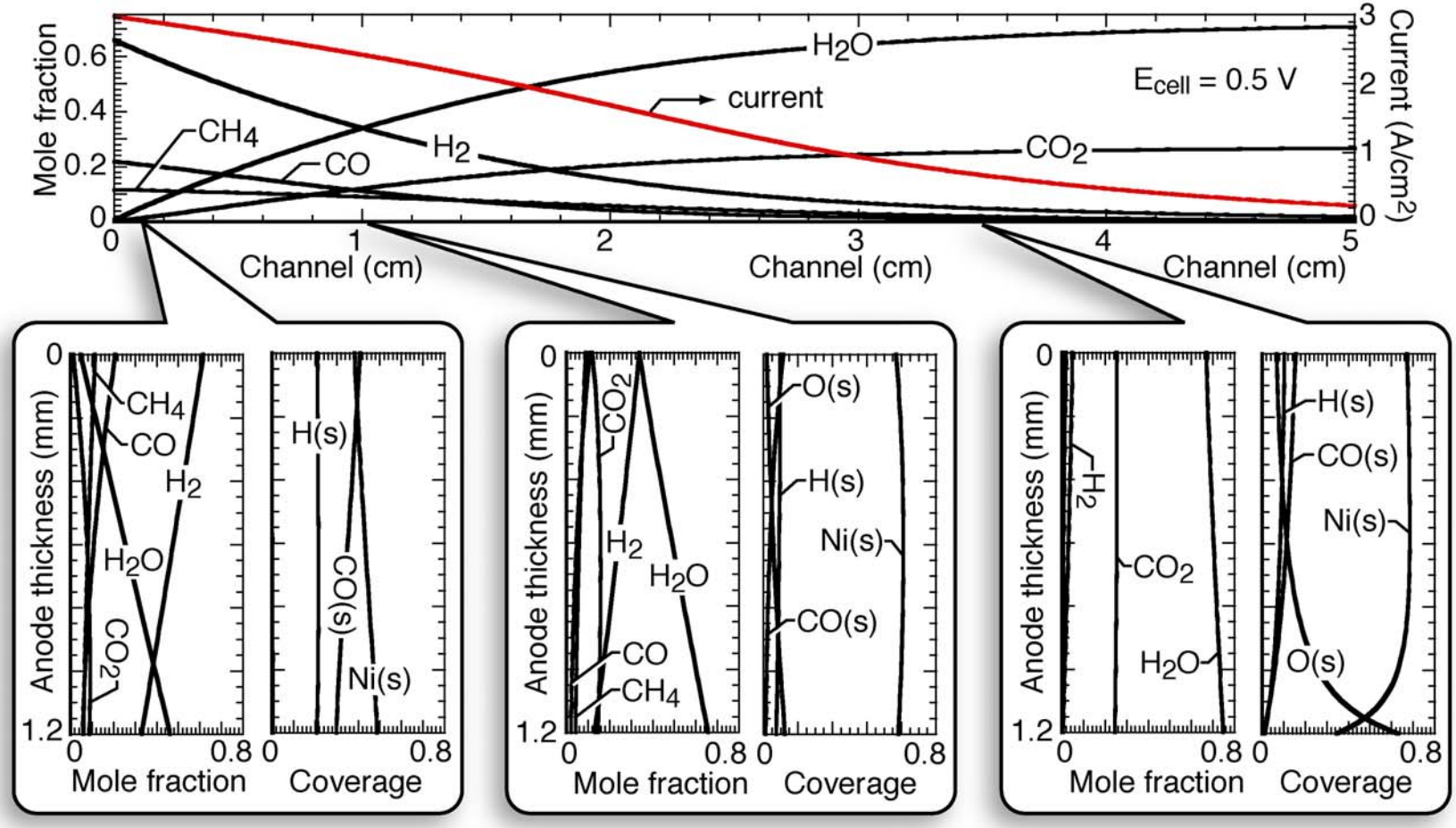

Anode Inlet: 66% H_2, 22% CO, 12% CH_4, 30 cm/s, 800˚C, 1 atm.
Cathode: Air

Efficiency, utilization, and power density depend greatly on operating voltage

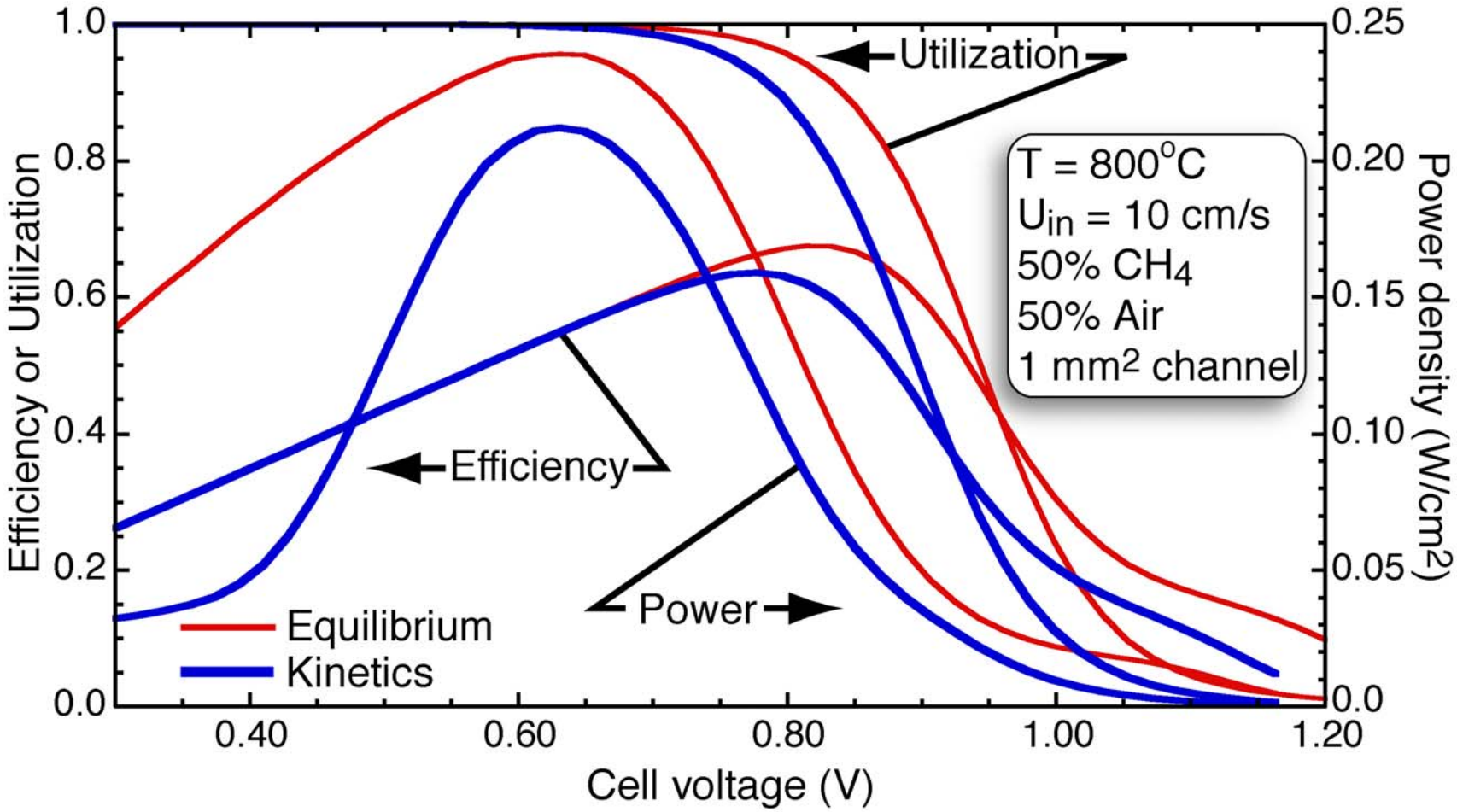

Although understanding is advancing rapidly, much remains to be done

Charge-transfer chemistry

- Currently in modified BV form ==> Need elementary mechanisms
- Currently consider H2 ==> Need general mixed potential
- Limited validation data ==> Need validation data and theory

Reforming and CPOX chemistry

- Current models for methane ==> Need higher hydrocarbons
- Current models for Ni ==> Consider alternative catalysts
- Assume inert ceramic supports ==> Investigate ceramic activity

Cell and electrode optimization

- Structure drives performance ==> Functionally grade electrodes
- Alternative catalyst function ==> Functionally grade electrodes

Coupling at the stack and system level

- Models are for single channel ==> Extend to full cell and stack
- Couple to thermal analysis ==> Depends on system boundaries
- Models for channels ==> Consider tube or sheet layout